Measurement of the longitudinal momentum distribution of ^{30}S after one-proton removal from ^{31}Cl

Y. Fu,[1] D. Q. Fang,[1,*] Y. G. Ma,[1] X. Z. Cai,[1] W. D. Tian,[1] H. W. Wang,[1] W. Guo,[1] G. H. Liu,[1] C. W. Ma,[1,†] R. R. Fan,[2] F. Fu,[2] H. Gao,[2] Q. Gao,[2] W. T. Guo,[2] J. L. Han,[2] Z. G. Hu,[2] T. H. Huang,[2] F. Jia,[2] B. Li,[2] X. G. Lei,[2] Z. Y. Sun,[2] M. Wang,[2] J. S. Wang,[2] Z. G. Xiao,[2,‡] Z. G. Xu,[2] X. W. Yao,[2] H. B. Zhang,[2] X. H. Zhang,[2] C. Zheng,[2] H. S. Xu,[2] G. Q. Xiao,[2] and W. L. Zhan[2]

[1]*Shanghai Institute of Applied Physics, Chinese Academy of Sciences, Shanghai 201800, China*

[2]*Institute of Modern Physics, Chinese Academy of Sciences, Lanzhou 730000, China*

(Received 13 June 2011; revised manuscript received 8 August 2011; published 15 September 2011)

The breakup reactions of ^{31}Cl + ^{12}C at 44A MeV are investigated experimentally. The longitudinal momentum distribution of ^{30}S after one-proton removal from ^{31}Cl has been obtained. By assuming core plus a valence proton structure, the momentum distribution is studied using the few-body Glauber model. The calculation shows that the width of momentum distribution for a valence proton with $l = 2$ is consistent with the experimental data, which indicates a dominant d-wave component for the valence proton in ^{31}Cl.

DOI: 10.1103/PhysRevC.84.037603 PACS number(s): 25.60.−t, 21.60.−n, 27.30.+t

Since the discovery of halo structure in ^{11}Li [1,2], study of the exotic structure of nuclei far from the β-stability line has become one of the frontiers of nuclear physics. The neutron halo is a structure with a dilute neutron distribution which extends far beyond the core of the nucleus. The structure of unstable nuclei has been investigated extensively with the development of radioactive ion beam techniques. The reaction cross section (σ_R) and fragment momentum distribution after one-nucleon removal have been widely used to investigate the exotic structure of nuclei both experimentally and theoretically [1–8]. As shown in the Glauber model [9], σ_R is directly related to the matter distribution of a nucleus. It has been widely used to extract the size of nuclei. The density distribution of a valence nucleon in halo nuclei will be much different from that of a nucleon inside the core. According to the uncertainty principle of quantum mechanics, the momentum distribution of the valence nucleon reflects its spatial distribution. The longitudinal momentum distribution of the fragment ($P_\parallel$) is one of the most sensitive observables for investigating the configuration of the valence nucleon. The halo structures of ^{11}Li, ^{11}Be, etc. have been established through experimental measurements of such observations [1,2,5–8].

During the past few decades, a large number of neutron halos have been reported [10,11]. However, studies on the proton halo have been relatively rare. Compared with the neutron halo, the proton halo is more difficult form due to the Coulomb repulsion interaction. Some experimental investigations indicated the existence of a proton halo in the light proton-rich nuclei ^{8}B, ^{17}Ne, and the first excited state of ^{17}F, etc. [12–17]. For heavier proton-rich nuclei, several experiments have been done to study the exotic structure in ^{23}Al and ^{26,27}P [18–23].

The separation energy of the last proton in ^{31}Cl is very small (0.294 MeV) [24]. A tail appears in the calculated proton density distribution of ^{31}Cl by the relativistic mean-field model and relativistic density-dependent Hartree theory [25]. So there may exist an exotic proton distribution structure in ^{31}Cl. But no enhancement of the interaction cross section for ^{31}Cl has been observed at high energy [26]. Therefore, further experimental study on ^{31}Cl is significant for our understanding its structure, especially measurement of the fragment momentum distribution, which could determine the orbit of its valence proton. Based on the time-of-flight (TOF) method, the longitudinal momentum distribution of ^{30}S after one-proton removal from ^{31}Cl at 44A MeV has been measured. In this Brief Report, we will present the experimental results and also discuss the structure of ^{31}Cl determined by the data.

The experiment was performed at the Heavy Ion Research Facility in Lanzhou (HIRFL). Secondary beams were produced by the Radioactive Ion Beam Line in Lanzhou (RIBLL) through the projectile fragmentation of an 82A MeV ^{36}Ar primary beam delivered by HIRFL. The experimental setup is shown in Fig. 1. The Be production target (0.5 mm) was mounted at the target chamber (T0). From T0 to the first achromatic focal plane T1, RIBLL can be used as an achromatic magnetic spectrometer where the exotic nuclei produced in the primary reaction, such as ^{31}Cl, were separated and selected by means of magnetic rigidity ($B\rho$) and an Al degrader (200 mg/cm^2) placed at the first dispersive focal plane C1. After passing through the degrader, the ^{31}Cl beams were focused onto T1 where the carbon reaction target (1 mm) was placed. Before the C target, two parallel plate avalanche counters (PPACs) were used to determine the beam position and incident angle. A plastic scintillator was placed between the two PPACs to measure the TOF from T0 (rf of the accelerator as the start signal). After the second PPAC, a silicon detector (300 μm thick) was used to measure the energy loss (ΔE) of the incident beam. The particle identification for the incident ^{31}Cl before the reaction target was made by the $B\rho$-ΔE-TOF method. After the beam passes through the position and incident angle gates, the purity of ^{31}Cl is estimated to be 99.5%.

After the reaction target, particles were identified by the TOF-ΔE-E method. A PPAC was installed at the second

*dqfang@sinap.ac.cn

†Present address: Henan Normal University, Xinxiang, Henan 453007, China.

‡Present address: Tsinghua University, Beijing 100084, China.

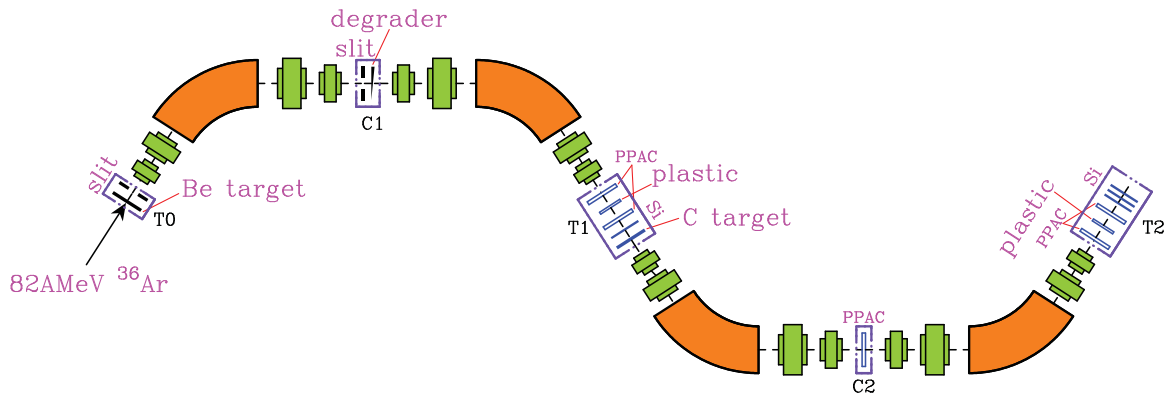

FIG. 1. (Color online) Experimental setup at the Radioactive Ion Beam Line in Lanzhou (RIBLL).

dispersive focal plane C2, which is only used for beam tuning. At the second achromatic focal plane T2, two PPACs were installed. Another plastic scintillator was placed between the two PPACs. The TOF between T1 and T2 was determined by the two plastic scintillators. A telescope was installed after the second PPAC at T2, which consisted of three silicon detectors (with 150-, 300-, and 300-μm thicknesses). In the measurement, ^{31}Cl and ^{30}S fragments were stopped in the third Si detector. For particle identification, the sum of the energy loss in the first and second Si detectors was used as the ΔE signal. The energy loss in the third detector was used as the E signal. The particle identification of ^{30}S fragments from ^{31}Cl after one-proton removal was done in two steps. First, the correlation between ΔE and E was used to identify charge. Second, the TOF-E correlation was used for mass identification. With the two-step identification, the ^{30}S fragments from ^{31}Cl breakup could be well identified [25,27,28].

The longitudinal momentum distributions of ^{30}S fragments from ^{31}Cl breakup were determined by the TOF between T1 and T2 at RIBLL as in the previous experiment [28]. Under the assumption of a sudden valence-nucleon removal, the momentum distribution of fragments after one-proton removal can be used to describe that of the valence proton. In the present experiment, the momentum of fragments was determined from the velocity (or TOF) between T1 and T2 measured by the plastic scintillators. Using a Lorentz transformation, the fragment momentum in the laboratory frame was transformed into that in the projectile rest frame, $p = \gamma(p_{\rm lab} - \beta E_{\rm lab})$, where $p_{\rm lab}$ and $E_{\rm lab}$ are, respectively, the momentum and energy of the fragment in the laboratory frame, and β and γ are the relativistic β and γ of the incident projectile in the laboratory frame, which was determined by the measured $B\rho$ value of the second dipole after considering the energy loss in the detectors before the C reaction target.

Figure 2 shows the experimental result of the longitudinal momentum distribution of ^{30}S fragments from ^{31}Cl breakup in the carbon target. The energy of the projectile ^{31}Cl at the center of the C target is 44A MeV. A Gaussian function was used to fit the $P_{\parallel}$ distribution. Since the measured $P_{\parallel}$ distribution of ^{30}S includes the broadening effect of the C target, this effect was simulated by using the MOCADI code [29]. The measured $B\rho$ value is used in the simulation. Assuming that the reaction takes place in the middle of the target, one can obtain the width of $P_{\parallel}$ without the broadening effect of the C target by requiring that the simulated $P_{\parallel}$ of ^{30}S after the C target be the same as that of the experimental data. The final full width at half maximum (FWHM) of $P_{\parallel}$ was determined to be 158 ± 40 MeV/c. The uncertainty includes the statistical error and the error from the MOCADI simulation for the uncertainty of the reaction position in the C target. From T1 to T2, the $B\rho$ value of the dipole magnets is optimized for the fragment ^{30}S and the slit at C2 is full open. The effect of the loses due to angular and momentum acceptance on the width of the momentum distribution of ^{30}S is negligible based on the MOCADI simulation.

According to the shell model, the last proton in ^{31}Cl should be in the d wave. Due to the small separation energy of the last proton and deformation of ^{31}Cl, the inversion of s and d waves may be possible based on relativistic mean-field calculations [30]. Since the fragment momentum distribution is very sensitive to the density distribution of the valence nucleon, we performed a few-body Glauber model (FBGM) analysis for $P_{\parallel}$ of the ^{31}Cl $\rightarrow$ ^{30}S process to interpret the experimental momentum distributions [20]. In this model, a core plus valence proton structure is assumed for the projectile.

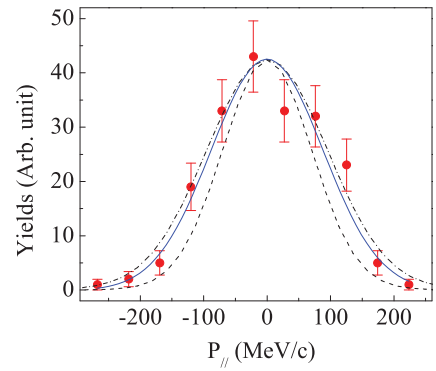

FIG. 2. (Color online) The longitudinal fragment momentum distribution of ^{30}S from ^{31}Cl after one-proton removal. The experimental data are shown by the dots. The solid line shows the Gaussian fit of the data. The dash and dash-dotted lines show the calculated momentum distribution of s and d waves by using the few-body Glauber model. For details see text.

The total wave function of the nucleus is expressed as

$$\Psi = \sum_{ij} \psi^i_{\rm core} \phi^j_0, \tag{1}$$

where $\psi_{\rm core}$ and ϕ_0 are wave functions of the core and valence proton, respectively, and i and j denote different configurations for the core nucleus and valence proton, respectively. For the core, harmonic oscillator (HO) functions were used for the density distributions. Since there are no experimental σ_R data for ^{30}S + ^{12}C and the effect of core size on the width of $P_\parallel$ is very small, the same value of the width parameter of ^{29}S is used by reproducing the σ_R data of ^{29}S + ^{12}C at 30A MeV [30]. The wave function of the valence proton was calculated by solving the eigenvalue problem in a Woods-Saxon potential [31],

$$\frac{d^2R(r)}{dr^2} + \frac{2\mu}{\hbar^2}\left[E - U(r) - \frac{l(l+1)\hbar^2}{2\mu r^2}\right]R(r) = 0,$$
$$U(r) = -V_0 f(r) + V_{ls}(\mathbf{l}\cdot\mathbf{s})r_0^2 \frac{1}{r}\frac{d}{dr} f(r) + V_{\rm Coul}, \tag{2}$$

where $f(r) = [1 + \exp(\frac{r-R}{a})]^{-1}$ with $R = r_0 A_c^{1/3}$ (V_{ls} = 17 MeV), V_0 is the depth of potential, and $V_{\rm Coul}$ is the Coulomb potential. In the calculation, the diffuseness (a) and radii parameter (r_0) were chosen to be 0.67 and 1.27 fm, respectively [20]. The separation energy of the last proton in ^{31}Cl is reproduced by adjusting the potential depth V_0. From the wave function, the density of the valence proton is deduced. The calculated matter density distributions for the core and ^{31}Cl in the s and d waves are shown in Fig. 3. The valence proton density distributions are also shown in the inset. For the valence proton in the s wave, the tail of the density is much longer than that of the d wave.

With the obtained wave functions, the momentum distributions for the valence proton in the s- or d-wave configuration are calculated using FBGM [32,33]. To compare the calculation with the present data, the broadening effect of the reaction target should be considered. After considering this

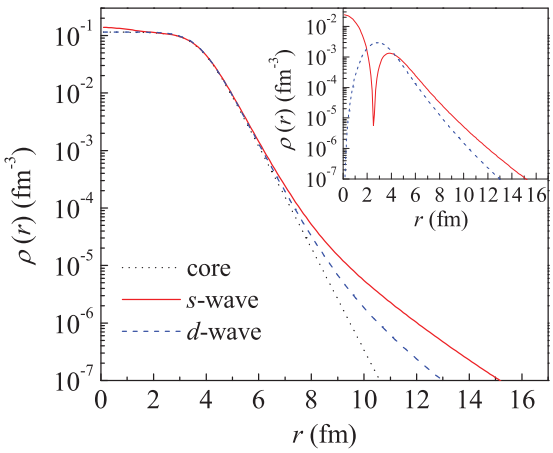

FIG. 3. (Color online) The density distribution of ^{31}Cl. The matter distribution for the core of ^{31}Cl is shown by the dotted line. The matter distribution of ^{31}Cl for the valence proton in s wave and d waves are shown by the solid and dashed lines, respectively. The corresponding valence proton density distributions are shown in the inset.

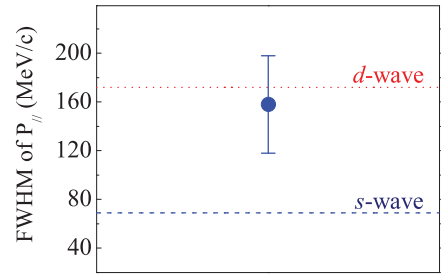

FIG. 4. (Color online) The FWHM of the momentum distribution of ^{30}S from ^{31}Cl after one-proton removal. The dot is the experimental datum. The dashed and dotted lines refer to the FWHM value of s and d waves, respectively.

effect based on the MOCADI simulation mentioned above, we plot the momentum distributions for s and d waves in Fig. 2. In this figure, the peak values of s and d waves are normalized to that of the fitted Gaussian function. We can see that the data are much closer to the shape of the d wave than to that of the s wave. Since the width is the most important parameter for describing the property of momentum distribution, for the d wave, the FWHM of $P_\parallel$ is found to be 172 MeV/c by using a Gaussian fit and, for the s wave, both Gaussian and Lorentzian functions fail to fit the calculated results well. The direct full width at half of the peak value (69 MeV/c) is used as its FWHM. As shown in Fig. 4, the width of the s wave is much smaller than that of experimental $P_\parallel$ data, whereas the width of the d wave is consistent with the data within the uncertainty. Thus the FBGM analysis indicates that the valence proton of ^{31}Cl should be dominantly in the d-wave configuration, which is the normal shell-model orbit. This result is consistent with the interaction cross section data at high energy, which shows no increase for ^{31}Cl compared with other $A = 31$ nuclei [26].

In summary, the one-proton removal reaction of 44A MeV ^{31}Cl + ^{12}C was studied at the Radioactive Ion Beam Line in Lanzhou. The longitudinal momentum distribution of the ^{30}S fragment after one-proton removal from ^{31}Cl was measured. Assuming a core plus proton structure for ^{31}Cl, we performed a few-body Glauber model analysis. The calculation shows that the width of the momentum distribution for a proton in an $l = 2$ orbit is consistent with the measured $P_\parallel$ data, which suggests a dominant d wave for the valence proton in ^{31}Cl as predicted by the shell model. This result is in accordance with the interaction cross section data measured at high energy.

We would like to thank the members of the RIBLL group and the HIRFL staff for all their support and excellent operation of the facility in delivering the ^{36}Ar beam and tuning of ^{31}Cl. This work was supported by the National Natural Science Foundation of China under Contracts Nos. 10775168, 10979074, 10975174, and 11035009, the Major State Basic Research Development Program in China under Contract No. 2007CB815004, the Shanghai Development Foundation for Science and Technology under Contract No. 09JC1416800, and the Knowledge Innovation Project of CAS under Grant No. KJCX2-EW-N01.

[1] I. Tanihata *et al.*, Phys. Rev. Lett. **55**, 2676 (1985).
[2] I. Tanihata *et al.*, Phys. Lett. B **287**, 307 (1992).
[3] E. Sauvan *et al.*, Phys. Rev. C **69**, 044603 (2004).
[4] P. G. Hansen and J. A. Tostevin, Annu. Rev. Nucl. Part. Sci. **53**, 219 (2003).
[5] T. Kobayashi *et al.*, Phys. Rev. Lett. **60**, 2599 (1988).
[6] M. Fukuda *et al.*, Phys. Lett. B **268**, 339 (1991).
[7] D. Bazin *et al.*, Phys. Rev. Lett. **74**, 3569 (1995).
[8] A. Ozawa *et al.*, Nucl. Phys. A **691**, 599 (2001).
[9] R. J. Glauber, *Lectures in Theoretical Physics*, Vol. 1 (Interscience, New York, 1959).
[10] P. G. Hansen *et al.*, Annu. Rev. Nucl. Part. Sci. **45**, 591 (1995).
[11] B. Jonson, Phys. Rep. **389**, 1 (2004).
[12] T. Minamisono *et al.*, Phys. Rev. Lett. **69**, 2058 (1992).
[13] W. Schwab *et al.*, Z. Phys. A **350**, 283 (1995).
[14] R. E. Warner *et al.*, Phys. Rev. C **52**, R1166 (1995).
[15] F. Negoita *et al.*, Phys. Rev. C **54**, 1787 (1996).
[16] M. Fukuda *et al.*, Nucl. Phys. A **656**, 209 (1999).
[17] M. M. Obuti *et al.*, Nucl. Phys. A **609**, 74 (1996).
[18] A. Navin *et al.*, Phys. Rev. Lett. **81**, 5089 (1998).
[19] X. Z. Cai *et al.*, Phys. Rev. C **65**, 024610 (2002).
[20] D. Q. Fang *et al.*, Phys. Rev. C **76**, 031601R (2007).
[21] A. Ozawa *et al.*, Phys. Rev. C **74**, 021301(R) (2006).
[22] T. Nagatomo *et al.*, Hyperfine Interact. **198**, 103 (2010).
[23] A. Gade *et al.*, Phys. Rev. C **77**, 044306 (2008).
[24] G. Audi and A. H. Wapstra, Nucl. Phys. A **729**, 337 (2003).
[25] X. Z. Cai *et al.*, Chin. Phys. Lett. **19**, 1068 (2002), and references therein.
[26] A. Ozawa *et al.*, Nucl. Phys. A **709**, 60 (2002).
[27] D. Q. Fang *et al.*, Eur. Phys. J. A **12**, 335 (2001).
[28] Y. B. Wei *et al.*, Chin. Phys. Lett. **22**, 61 (2005).
[29] N. Iwasa *et al.*, Nucl. Instrum. Methods B **126**, 284 (1997).
[30] H. Y. Zhang *et al.*, Nucl. Phys. A **707**, 303 (2002).
[31] J. Speth *et al.*, Phys. Rep. **33**, 127 (1977).
[32] Y. Ogawa *et al.*, Nucl. Phys. A **543**, 722 (1992).
[33] B. Abu-Ibrahim *et al.*, Comput. Phys. Commun. **151**, 369 (2003).